Journal of Electromyography and Kinesiology 48 (2019) 187–196

Contents lists available at ScienceDirect

Journal of Electromyography and Kinesiology

journal homepage: www.elsevier.com/locate/jelekin

Decomposing single-channel intramuscular electromyography signal sampled at a low frequency into its motor unit action potential trains with a generative adversarial network

Wentao Sun[a,b], Rongyu Tang[c,*], Yiran Lang[c], Jiping He[a], Huang Qiang[a]

[a] Key Laboratory of Biomimetic Robots and Systems, Ministry of Education, Beijing, China
[b] School of Mechatronical Engineering, Beijing Institute of Technology, Beijing, China
[c] Beijing Innovation Center for Intelligent Robots and Systems, Beijing, China

ARTICLE INFO

Keywords:
Generative adversarial network
Intramuscular electromyography decomposition
Motor unit action potential trains

ABSTRACT

Conventional methods decompose single-channel intramuscular electromyography (iEMG) signals into their constituent motor unit action potential trains (MUAPTs) by detecting and clustering individual motor unit action potentials (MUAPs). However, these methods are not applicable for iEMG signals recorded by electrodes with a large sensing areas or iEMG signals sampled at a low frequency, in which detecting and clustering individual MUAPs are difficult due to superimpositions of the MUAPs and the loss of MUAP morphological characteristics. In this study, we propose an approach based on a generative adversarial network to decompose iEMG signals, which does not depend on detecting and clustering individual MUAPs from the iEMG signal. The proposed approach decomposes the iEMG signal into its MUAPTs based on Bayes' law and a Wasserstein generative adversarial network with gradient penalty (WGAN-GP). MUAPTs generated by the WGAN-GP were used to decompose the iEMG signal to maximize the posterior probability of the generated MUAPTs given the iEMG signal. The accuracy of the proposed approach is analysed directly by decomposing the simulated iEMG signal with seven gold-standard motor units. The results showed that the proposed approach achieved a 53% accuracy in capturing the firing regularities of the MUs, while the conventional method achieved a 37% accuracy on the same task.

1. Introduction

Over the past several decades, intramuscular electromyography (iEMG) signal decomposition has drawn the attention of researchers from many fields. The attractiveness of iEMG signal decomposition lies in its observation the behaviour of individual motor units in the human nervous system (Mcgill et al., 2005). Motor unit activities, which reflect the neural strategies for muscle activation, have great potential in prosthetic limb control, rehabilitation performance evaluation, and neuromuscular disorder diagnosis. Originally, iEMG electrodes with small sensing areas were used to obtain motor unit action potential trains (MUAPTs) because of their spatial selectivity to detect individual motor unit action potentials (MUAPs) generated by the underlying motor units (MUs) (Adrian and Bronk, 1928). However, they provide limited information about activity at the whole-muscle level (Farina and Negro, 2015; Thompson et al., 2018). To obtain a global measure of muscle activation, researchers prefer electrodes with large sensing areas, such as macro needle electrodes. However, the signals from these electrodes are difficult to decompose due to the superimpositions of MUAPs caused by the large number of motor units detected by the electrodes (Lefever and Luca, 1982; Luca and Adam, 1999). In addition, to enhance the use of iEMG in real-world applications, researchers are developing implantable devices that wirelessly transfer iEMG signals (Mcdonnall et al., 2012; Weir et al., 2009; Bergmeister et al., 2017). iEMG used in these cases is usually sampled at a low frequency for wireless transfer. Therefore, conventional methods have difficulties in clustering MUAPs from the iEMG signals sampled at a low frequency due to the loss of the MUAP morphological characteristics.

iEMG signal decomposition can be considered a blind source separation problem, which aims to recover the MUAPTs (sources) from the sensor observations (EMG) (Negro et al., 2016; Zhu and Zhang, 2012). Currently, great advances have been achieved by researchers in decomposing surface electromyography (sEMG) signals recorded by multi-channel surface electrodes. For example, a convolution kernel compensation (CKC) method is proposed to decompose high-density sEMG signals (Holobar and Zazula, 2004; Holobar and Zazula, 2007) to

* Corresponding author.
E-mail address: tangrongyu@semi.ac.cn (R. Tang).

https://doi.org/10.1016/j.jelekin.2019.07.015
Received 16 January 2019; Received in revised form 10 July 2019; Accepted 30 July 2019

study the neural strategies of muscle activation. A novel framework based on fast independent component analysis (ICA) was proposed to extract large numbers of MUs from 64 channels of sEMG signals (Chen and Zhou, 2015), and an incremental approach based on machine learning and time-varying MUAP shape discrimination was proposed to decompose 4 channels of sEMG signals during repetitive dynamic contractions (De Luca et al., 2015). However, in contrast to the increase in multi-channel sEMG signal decomposition methods, less progress has been made in single-channel iEMG signal decomposition. The limited information provided by single-channel iEMG signals makes it impossible to use cross-channel correlations, which are commonly used in decomposing multi-channel sEMG signals. Conventional methods to decompose single-channel iEMG signals into its MUAPTs mainly consist of two steps: detecting MUAPs from iEMG signals and clustering the detected MUAPs into groups (MUAPTs). Currently, almost all of the methods for detecting MUAPs are based on defining some detection threshold by means of some statistics computed using the iEMG signal (Stashuk, 2001). Either fixed length or variable length segmentations of the detected MUAPs are used for clustering (Gerber et al., 1984; Loudon et al., 1992). Clustering of the detected MUAPs is based on features of the MUAPs. Morphological characteristics, for example, are one of the most widely used features for clustering MUAPs. Autoregressive coefficients, time-frequency analyses, and morphological statistics of the detected MUAPs are commonly used morphological characteristics for clustering MUAPs (Christodoulou and Pattichis, 1999; Mcgill et al., 1985; Stashuk and Bruin, 1988). In addition to morphological characteristics, firing (discharge) patterns of the MUAPs are other features commonly used to cluster the MUAPs (Etawil and Stashuk, 1996; Marateb et al., 2011). However, the accurate clustering of the MUAPs requires detecting enough individual MUAPs to determine the MUAP features for each group. Therefore, the MUAPs of each group have to occur enough times by themselves (i.e., not at the same time as the MUAPs of other groups), so that the respective features of MUAPs for each group can be determined (Stashuk, 2001). As a result, conventional methods are difficult to employ in decomposing low-frequency single-channel iEMG recorded by electrodes with large sensing areas, where the detected MUAPs have a high probability of being superimposed and morphological characteristics are lost due to the low sampling frequency.

In this paper, we propose an approach based on Bayes' law and a generative adversarial network to decompose a low-frequency single-channel iEMG signal into its constituent MUAPTs, which does not depend on detecting and clustering individual MUAPs as an intermediate step. A Wasserstein generative adversarial network with gradient penalty (WGAN-GP) was trained to generate MUAPTs. The proposed approach decomposes an EMG signal by maximizing the posterior probability of the generated MUAPTs given the iEMG. The power of the generative adversarial network (GAN) in unsupervised source separation has been validated on speech (Stoller et al., 2018) and singing (Subakan and Smaragdis, 2018), where the GAN is used to model the sources. The accuracy of the proposed approach is validated by decomposing simulated iEMG signal sampled at 1 kHz with seven gold-standard motor units (MUs).

2. Background

2.1. EMG model

A motor unit action potential (MUAP) is the pulse generated by a motor unit (MU) when the MU is activated or stimulated, and a sequence of MUAPs is known as the motor unit action potential train (MUAPT) (De Luca and Forrest, 1973). Based on physiology findings on muscles, EMG signals can be roughly modelled as the sum of the constituent MUAPTs convolved with their channel responses. All the anatomic properties of the MUAPTs (e.g., their location within the muscle and the fibre orientation), volume conductor properties (e.g., the thickness of the subcutaneous tissue), and the properties of the detection system (e.g., the shape and size of electrodes) are modelled by channel responses. From the literature (Holobar and Farina, 2014), an EMG signal is modelled as:

$$x(t) = \sum_{i=1}^{n} A_i(t) * h_i(t) + \xi(t), \tag{1}$$

where $*$ denotes the convolution, $A_i(t)$ is the channel response of an MU i, $h_i(t)$ is the MUAPT generated by MU i, and $\xi(t)$ is the background noise at time t. This time-dependent equation is a general description of the EMG model; however, this equation is difficult to use for decomposing an EMG signal in terms of its time variance and complexity (calculating convolution). For an EMG signal recorded over a short time period, we assume the stationarity and independence of the MUAPTs, and we simplify the channel response to a scalar denoting the average channel response in the time period. Therefore, an EMG signal recorded over a short time period can be depicted as:

$$x(t) = \sum_{i=1}^{n} A_i h_i(t) + \xi;\ t = 1, 2, ..T \tag{2}$$

where A_i is a scalar denoting the average channel response of an MU i and T is the short-time period. By simplifying A_i to a scalar, the convolution in Eq. (1) is replaced with multiplication. Eq. (2) is used in the rest of the paper as the EMG signal model, which is a time-invariant simplification of Eq. (1).

2.2. Bayes' Law for EMG Decomposition

Bayes' law describes the probability of an event based on prior knowledge of conditions that might be related to that event (EricZiegel, 1994). Bayes' law for decomposing an EMG signal is stated as follows:

$$\arg\max_h p\left(h\middle|x\right) = \arg\max_h \frac{p(x|h)p(h)}{p(x)}, \tag{3}$$

where x is the EMG, h is the constituent MUAPTs, and $p(x)$ is the distribution of the recorded EMG signal, which is an unknown constant determined by various uncontrollable factors. The goal of EMG signal decomposition is to find the optimum decomposed MUAPTs that maximize the posterior probability of the MUAPTs given the EMG signal, namely, solving the left part of Eq. (3). However, solving the left part of the equation is hard due to the lack of a model for directly decomposing the EMG signal. Fortunately, Bayes' law provides an alternative way by solving the right part of Eq. (3). $p(x|h)$ on the right part of the equation is modelled by the EMG model described in Eq. (2), and $p(h)$, the probability of the occurrence of the MUAPTs, is modelled by an adversarial model introduced in the next subsection. In summary, our proposed approach solves the EMG signal decomposition problem (left part of Eq. (3)) by solving the alternative combined problem (right part of Eq. (3)). In the following subsection, some knowledge about the adversarial model is introduced.

2.3. GAN

A GAN is a framework for establishing a generative model via an adversarial process (Goodfellow et al., 2014), and it has been successfully used to model and analyse different types of data, such as images (Radford et al., 2015), noisy speech (Pascual et al., 2017), and languages (Rajeswar et al., 2017). A GAN is composed of two networks, a discriminator and a generator, and these two networks compete against each other to learn. The discriminator decides whether an instance is from the training set or was generated by the generator, while the generator tries to fool the discriminator by generating instances similar to those in the training set. The whole network learns through this competition. While a GAN has the power to handle a wide range of previously unsolved problems, it is notorious for its training difficulty

(Yadav et al., 2017). Training a GAN drives the network to a saddle point in the parameter space. Approaching the saddle point makes training a GAN very unstable. The discriminator and the generator can easily overwhelm each other and collapse the training process (Che et al., 2016).

The Wasserstein generative adversarial network with gradient penalty (WGAN-GP) (Arjovsky et al., 2017; Gulrajani et al., 2017) is an improvement over the original GAN to stabilize training. The main difference between a WGAN-GP and a GAN lies in their loss function. The loss functions of a WGAN-GP and a GAN evaluates the Wasserstein distance and Jensen-Shannon (JS) distance between the training set and the generated set, respectively. However, the JS distance is a constant when the training set and the generated set are disjoint, making the gradient of the loss function zero and training of the GAN collapse. In contrast, the Wasserstein distance provides a smooth measure even when the training set and the generated set are located in lower-dimensional manifolds without overlaps (Mueller and Jaakkola, 2015), which is helpful for a stable learning process using backpropagation. The loss function of WGAN-GP is:

$$\begin{aligned} L^1 &= E_{x\sim P_{data}}[D(h) - D(G(z))] + E_{x\sim P_G}[-D(G(z))] \\ L^2 &= \lambda\, E_{\hat{x}\sim P_{\hat{x}}}[(||\nabla_{\hat{x}} D(\hat{h})||_2 - 1)^2] \\ L^w &= L^1 + L^2 \end{aligned} \tag{4}$$

where L^w is the loss function of the WGAN-GP, L^1 denotes the Wasserstein distance, L^2 denotes the penalty to regularize the gradient, $\hat{h}$ is a random instance, $||\nabla_{\hat{h}} D(\hat{x})||_2$ is the gradient norm, and λ is the penalty coefficient. In practice, $\hat{h}$ is chosen as the interpolation between two instances from the training set and the generated set.

A WGAN-GP is used to generate MUAPTs because it is considered stable, robust, and easy to train (Arora and Zhang, 2017). In the methods section, we will show how to use the generated MUAPTs to decompose an EMG signal based on Bayes' law.

3. Methods

The proposed approach to decompose an EMG signal is composed of two steps: first, a WGAN-GP is trained to learn how to generate MUAPTs; second, the EMG signal is decomposed by MUAPTs generated from the WGAN-GP based on Bayes' law.

3.1. Datasets

To train the WGAN-GP to generate MUAPTs, datasets of MUAPTs are needed. The publicly available R001 and R005 (McGill, 2015) datasets were used, which contain iEMG signals from biceps brachii recorded with monopolar needles. The recorded iEMG signal was manually decomposed into its constituent MUAPTs using EMGLAB (Mcgill et al., 2005). Then, the manually decomposed MUAPTs were down-sampled to 1 kHz, put through a high-pass filter at 100 Hz, and segmented with a sliding window of 512 ms. To augment the data, the overlap of the sliding window is uniformly sampled from 0–512 ms. The MUAPTs were normalized to $-1 \sim 1$ before feeding them to the WGAN-GP.

3.2. WGAN-GP

The proposed WGAN-GP is designed with multiple hidden layers to extract complex features from the 1D time series of MUAPTs. Both the discriminator and the generator of the WGAN-GP are composed of nine hidden layers, as shown in Fig. 1. Each hidden layer of the discriminator consists of a one-dimensional convolution layer with a kernel size of 2 and stride 2 and a LeakyReLU activation layer with negative slope of 0.2. Each hidden layer of the generator consists of a one-dimensional transposed convolution layer with a kernel size of 2 and stride 2, a one-dimensional batch normalization layer, and a ReLU activation layer. The batch normalization layers are incorporated to improve the stability of the generator, which can regularize the direction and value of the gradient of the generator during backpropagation (Xiang and Li, 2017). With the normalization technique, the gradient of the WGAN-GP is less sensitive to the configuration of hyper-parameters, which reduces the risk of model collapse during training.

Although the architecture of the proposed WGAN-GP is carefully designed to stabilize its gradient, it still suffers from a high risk of collapse when trained at high learning rates with popular optimizers, such as stochastic gradient descent or Adam optimizers. These optimizers switch between minimization and maximization steps, and the training path of the WGAN-GP has a high possibility to "slide off" the saddle, and the loss goes to $-\infty$. To reduce the risk of collapsing, an Adam optimizer with prediction (Yadav et al., 2017) is adopted, which is asymptotically stable for a class of saddle point problems. Based on the prediction method, the parameters of the WGAN-GP are updated as follows:

$$\begin{aligned} u^{k+1} &= u^k - \alpha_g \nabla_u L^{w-gp}(u^k, v^k) \\ \bar{u}^{k+1} &= u^{k+1} + (u^{k+1} - u^k) \\ v^{k+1} &= v^k + \alpha_d \nabla_v L^{w-gp}(\bar{u}^{k+1}, v^k), \end{aligned} \tag{5}$$

where k is the k-th step of the iteration, α_g is the learning rate of the generator, and α_d is the learning rate of the discriminator. The parameter v is updated by predicting where u will be in the future. This prediction method guarantees that the training path of the GAN converges to the saddle point asymptotically by incorporating damping into the training path. A rigorous mathematical proof is presented in (Yadav et al., 2017).

3.3. EMG decomposition

In this subsection, the approach to decomposing an EMG signal based on MUAPTs generated by a WGAN-GP is introduced. As mentioned above, the decomposition is realized by solving the right part of Eq. (3). Note that $p(x)$ is considered a constant irrelevant to the decomposition, and we assumed the independence of the MUAPTs. We took the logarithm of both sides of Eq. (3), which does not influence the decomposition results, transforming the equation to

$$\begin{aligned} \arg\max_h \log\left[p\left(x\middle|h\right)p(h)\right] &= \arg\max_{h_1,\ldots,h_n}\left[\log p\left(x\middle|h_1,\ldots,h_n\right)\right. \\ &\left. + \sum_{i=1}^{n} \log p(h_i)\right] \end{aligned} \tag{6}$$

Now, the decomposition is transformed into Eq. (6). For MUAPTs generated by feeding a batch of uniformly distributed noise over $[-1, 1]$ to the trained WGAN-GP, finding MUAPTs to maximize the right part of Eq. (6) is equivalent to minimizing the loss function e shown below:

$$\begin{aligned} e &= \arg\min_{\hat{A}_i,\hat{z}_i}\left[-\phi_0 \log e^{-||x-\hat{x}||_2} - \phi_1 \sum_{i=1}^{b} \log D(\hat{h}_i) + \phi_2 \sum_{i=1}^{b} \left|\hat{A}_i\right|\right],\ \hat{x} \\ &= \sum_{i=1}^{b} \hat{A}_i \hat{h}_i,\ \ \hat{h}_i = G(\hat{z}_i);\ i = 1,\ \ldots, b \end{aligned} \tag{7}$$

where x is the EMG signal to be decomposed, $\hat{x}$ is the approximated EMG signal formed by the MUAPTs generated from the WGAN-GP multiplied by the channel responses, ϕ_0, ϕ_1 and ϕ_2 are penalties for regulating the minimization, b is the batch size denoting the number of MUAPTs expected, $\hat{h}_i$ is the generated MUAPT, $\hat{A}_i$ is the channel response of MUAPT i, and $\hat{z}_i$ is the input uniform noise of MUAPT i. $e^{-||x-\hat{x}||_2}$ is used to evaluate the probability of the EMG signal given the MUAPTs $p(x|\hat{h}_1, \ldots, \hat{h}_b)$. $e^{-||x-\hat{x}||_2}$ equals 1 while $\hat{x}$ matches x perfectly, and it approaches 0 while x and $\hat{x}$ differ significantly. The probability of occurrence of the generated MUAPTs $p(\hat{h}_i)$ is evaluated by $D(\hat{h}_i)$. The

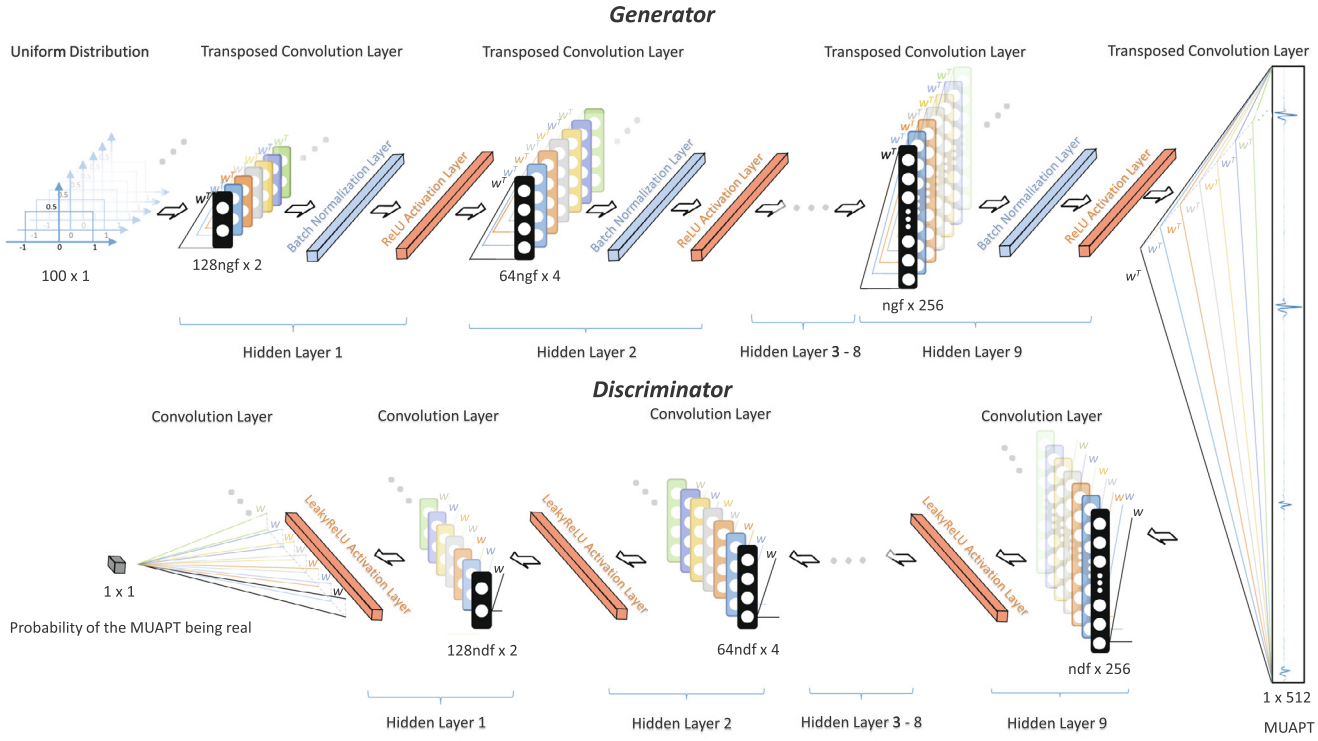

Fig. 1. Sketch of the layers used in the WGAN-GP. Both the generator and the discriminator are composed of 9 hidden layers. A hidden layer of the generator is composed of a transposed convolution layer, a batch normalization layer, and a ReLU activation layer. A hidden layer of the discriminator is composed of a convolution layer and a LeakyReLU activation layer. *ngf* and *ndf* in the figure represent the number of transformation channels in the transposed convolution layer and the convolution layer, respectively. ($ngf = ndf = 64$).

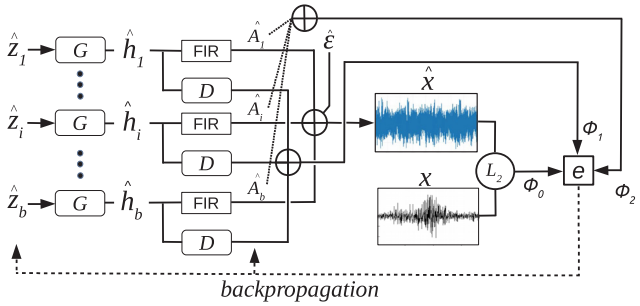

Fig. 2. Framework of the proposed iEMG decomposition approach. $\hat{z}_i$ is the input (uniform) noise. $\hat{A}_i$ is the channel response. $\hat{\xi}$ is the background noise. x and $\hat{x}$ represent the iEMG signal and its approximation, respectively. e is the loss function. G and D represent the generator and the discriminator of the WGAN-GP, respectively. *FIR* is the 100 Hz high-pass filter. L_2 outputs the mean squared error between x and $\hat{x}$. ϕ_0, ϕ_1 and ϕ_2 are the penalties. $\hat{z}_i$ and $\hat{A}_i$ are updated to minimize the loss function e through backpropagation.

probability of occurrence of the generated MUAPTs increases with the probability of the generated MUAPTs being real, as judged by the discriminator. Penalties ϕ_0 and ϕ_1 are used to change the focus of the optimization on approximating the EMG signal or on generating realistic MUAPTs. To reduce the loss e, a large batch size b is preferred to search a wide range of the variable space; however, this process will make the generated MUAPTs fit every detail in the EMG signal, even the background noise. To cope with this problem, $\phi_2 \sum_{i=1}^{b} |\hat{A}_i|$ is used as a penalty in sparse channel responses to retain the MUAPTs that contribute significantly to the EMG signal. Details about the influences of the penalties on the decomposition results are presented in the results section.

In this paper, Eq. (7) is used as a substitution of Eq. (6) to decompose EMG signals. The optimization of variables $\hat{z}$ and $\hat{A}$ is based on momentum gradient descent to navigate smaller errors. Updating the variables is as follows:

$$\begin{aligned}
\Delta\hat{z}_i^k &= \gamma\Delta\hat{z}_i^{k-1} + \alpha\nabla_{\hat{z}_i}e^k \\
\Delta\hat{A}_i^k &= \gamma\Delta\hat{A}_i^{k-1} + \alpha\nabla_{\hat{A}_i}e^k \\
\hat{z}_i &= \hat{z}_i - \Delta\hat{z}_i^k \\
\hat{A}_i &= \hat{A}_i - \Delta\hat{A}_i^k,
\end{aligned} \tag{8}$$

where α is the learning rate, γ is the momentum, and k is the optimization step. The optimization is terminated after 5000 steps. The optimized variables are denoted by $\hat{z}^O$ and $\hat{A}^O$.

The approximated background noise $\hat{\xi}$ is calculated by:

$$\hat{\xi} = y - \hat{A}^O\hat{h}^O \tag{9}$$

A trick we found for improving the performance of the decomposition is adding a 100 Hz high-pass FIR filter to the MUAPTs generated by the WGAN-GP. A FIR filter is used instead of an IIR filter because of its simplicity in forming a dense layer of the network. The FIR filter is used to fit the power spectrum of the MUAPTs to the iEMG signal, which is filtered with a 100 Hz high-pass filter to remove low-frequency noise. The framework of iEMG signal decomposition is shown in Fig. 2.

The approach introduced above is designed for decomposing the 512 ms iEMG signal segment. In a time series of the iEMG signal, the iEMG signal is segmented at a length of 512 ms, and each segment is decomposed with the proposed approach.

4. Experiments

The performance of the proposed approach is validated by decomposing the simulated iEMG signal with gold-standard MUs, which are used as references for testing the accuracy of the approach. The accuracy of the proposed approach is evaluated by comparing the firing time of the generated MUAPTs to that of the gold-standard MUs. The

simulated iEMG signal is the publicly available S002 dataset (Hamilton and Stashuk, 2005), which contains approximately 31 s of simulated single-channel iEMG signals with seven gold-standard motor units. The first 30 s of the simulated iEMG signal was re-sampled at 1 kHz and segmented at a length of 512 ms. The segmented signals were decomposed via two strategies: (1) the peel-off strategy, in which the segment is peeled off by a generated MUAPT each time, and (2) the all-together strategy, in which multiple MUAPTs are decomposed simultaneously. The advantage of the peel-off strategy is that the user can adjust the results in each step of decomposition, increasing the accuracy of the decomposed MUAPTs. However, its disadvantage is that the peel-off strategy is time consuming because it requires running the decomposition multiple times. The advantage of the all-together strategy is that it is fast and requires fewer interactions with the user than the peel-off strategy. However, the all-together strategy allows the user to only reject or accept the generated MUAPTs after decomposition is finished. Therefore, the accuracy of the all-together strategy is often lower than that of the peel-off strategy. Furthermore, the simulated iEMG signal was also decomposed with the conventional approach based on the detecting and clustering individual MUAPs. MUAPs were detected if their amplitude exceeded a predefined threshold, and the detected MUAPs were clustered according to their shape characteristics using K-means clustering (Arthur and Vassilvitskii, 2007). The code for the conventional method used to decompose the simulated iEMG signals is available in the appendix.

5. Results

5.1. WGAN-GP

The proposed WGAN-GP is trained to generate MUAPTs based on the training set. Fig. 3 shows the loss of the generator and the discriminator during training. It is the trend of the loss instead of its value that accounts for the state of the training. The rapid decrease in the loss of the generator from epoch 200 to 400 shows that the discriminator and the generator are learning simultaneously. The final losses of the discriminator and the generator stabilize at approximately -1.7 and -0.3, and the training is terminated after 1000 epochs. In each epoch, instances generated by the generator were saved to check the state of the generator. Instances generated at epochs 10, 200, 400, 800, and 1000 are shown. The generator learns to generate realistic MUAPTs as the loss of the generator stabilizes.

To obtain an intuitive understanding of what the WGAN-GP learns, 32 random instances from the training set and 32 instances generated by the generator are shown in Fig. 4. From the figure, we can see that the generator learns that a MUAPT is a sequence of pulses arranged at regular intervals. The probability of the MUAPT being real (i.e., coming from the training set) according to the discriminator is shown in the middle of the figure, from which we can see that the inter-pulse interval is an important criterion used by the discriminator to assess the reality of the MUAPT. In fact, the inter-pulse interval of the MUAPT is considered an important way that the neural system encodes neural commands. To check whether the generator learns to model the intervals quantitatively, the inter-pulse interval distribution of the instances of the training set and generated by the generator are fitted with a gamma distribution. The shape parameter and the scale parameter of the gamma distribution of the training set are 2.20 and 20.26, respectively, while those of the generated set are 15.94 and 8.09, respectively. The area of overlap between the gamma distribution of the training set and the generated set is 0.8503, which means the generated set covers approximately 85% of the variability in the firing patterns of the training set. In addition, the generator also learns that the waveforms of the pulses in the MUAPT are similar.

5.2. Simulated iEMG signal decomposition

5.2.1. Influence of penalties

Penalties ϕ_0, ϕ_1, and ϕ_2 greatly influence the decomposition results. Fig. 5 shows the decomposition results of a single MUAPT (setting $b = 1$) from the simulated iEMG signal at different penalties and the probability of the MUAPT judged by the discriminator. The penalties [ϕ_0, ϕ_1, andϕ_2] for the decomposition are (a) [1,1,0], (b) [1,2,0], (c) [2,1,0], and (d) [1,1,1]. The probabilities of the decomposed MUAPTs being real,as judged by the discriminator, are (a) 0.8293, (b) 0.8578, (c) 0.8309, (d) 0.6883, and (e) 0.8416. From the figure, we can see that setting [ϕ_0, ϕ_1, ϕ_2] to [1,2,0] (b) achieves the best decomposition results according to the given gold-standard MU; however, the best decomposed MUAPT cannot match the gold-standard MU perfectly because the discriminator does not judge the gold-standard MU as the "best". The discriminator assigns a probability of 0.8416 to the gold-standard MU lower than 0.8578 of the best decomposed MUAPT. The discriminator trained with a few samples lacks full knowledge about the diverse patterns of the MUAPT. There are two ways to overcome this deficiency: one way is manually adjusting the decomposed MUAPT based on the decomposition results, and the other way is collecting more examples to train the WGAN-GP model.

5.2.2. Peel-off Strategy

Penalties ϕ_0, ϕ_1, and ϕ_2 are set to 1, 2, and 0 for the peel-off strategy. MUAPTs are peeled off one by one from the simulated iEMG, as shown in Fig. 6. From the figure, we can see that spike-like waveforms in the simulated iEMG signal are gradually eliminated by the generated MUAPTs. However, the generated MUAPTs cannot match the gold-standard MUs perfectly. The mismatched or false-matched MUAPTs will influence the decomposition of the next MUAPTs. The firing time of the generated MUAPTs is extracted by a simple threshold-based approach. The accuracy of the decomposed MUAPTs compared with the gold-standard MUs is 55% with 22 true positives, 8 false positives and 10 false negatives, as shown in Fig. 7. A True positive means there is a firing of the motor unit and the generated MUAPTs captures it, a false positive means there is not a firing of the motor unit but the generated MUAPTs captures one, and a false negative means there should be a

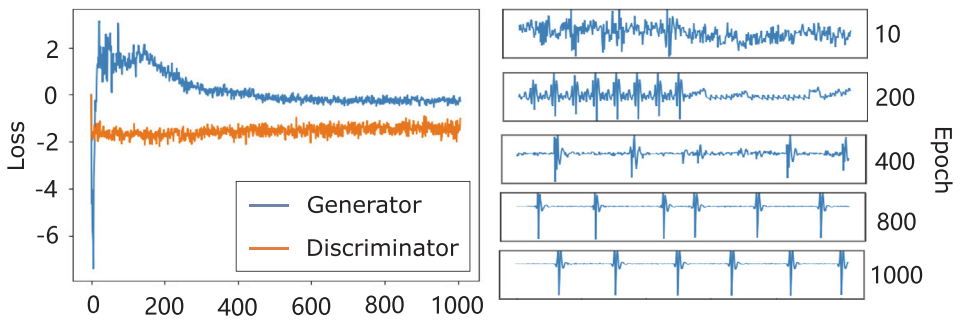

Fig. 3. Losses of the discriminator and the generator of the proposed Wasserstein generative adversarial network with gradient penalty and the MUAPTs generated at 10, 200, 400, 800, and 1000 epoch.

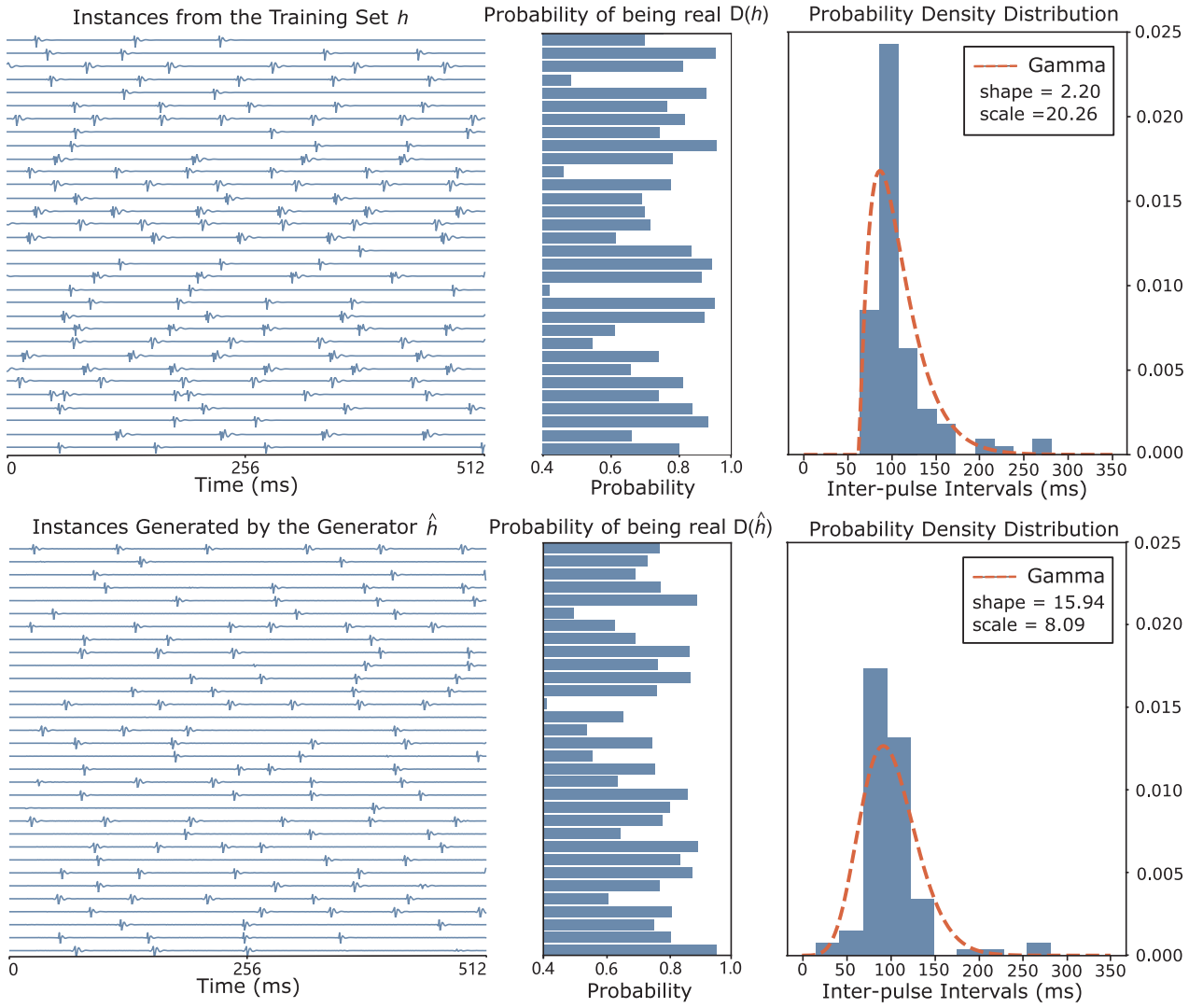

Fig. 4. Performance of the proposed WGAN-GP in modelling and generating MUAPTs. **Left**: each 32 randomly sampled MUAPTs from the training set and generated by the generator. **Middle**: probability of the generated MUAPTs being real, according to the discriminator. **Right**: inter-pulse interval distribution of the generated MUAPTs.

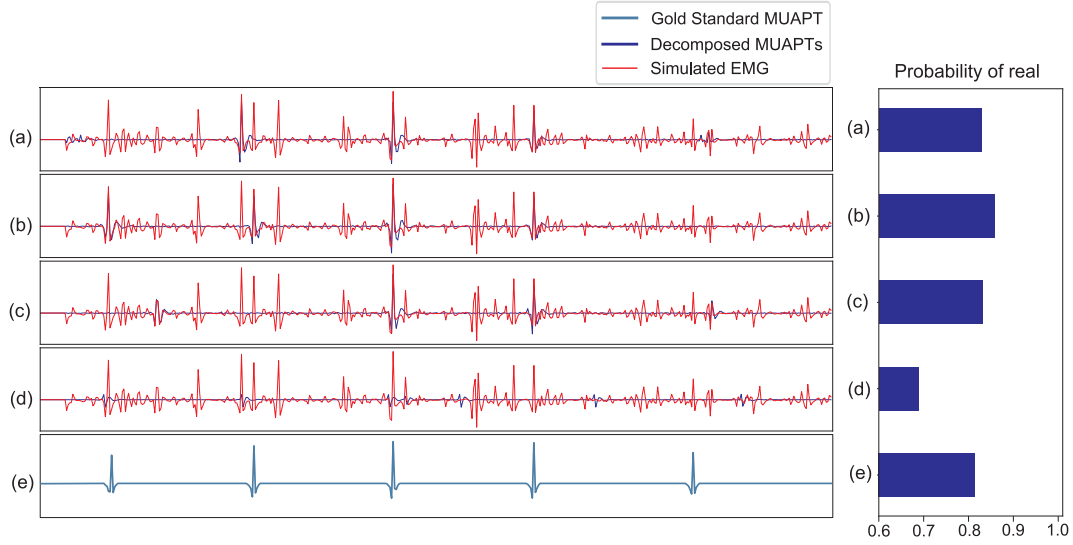

Fig. 5. Influences of the penalties on the decomposition results. **Left**: MUAPTs decomposed from simulated iEMG signal using different penalty values for [ϕ_0, ϕ_1, ϕ_2] (a) [1,1,0], (b) [1,2,0], (c) [2,1,0], and (d) [1,1,1]. (e) is the gold-standard MU. **Right**: Probability of the decomposed MUAPTs judged by the discriminator: (a) 0.8293, (b) 0.8578, (c) 0.8309, (d) 0.6883, and (e) 0.8146.

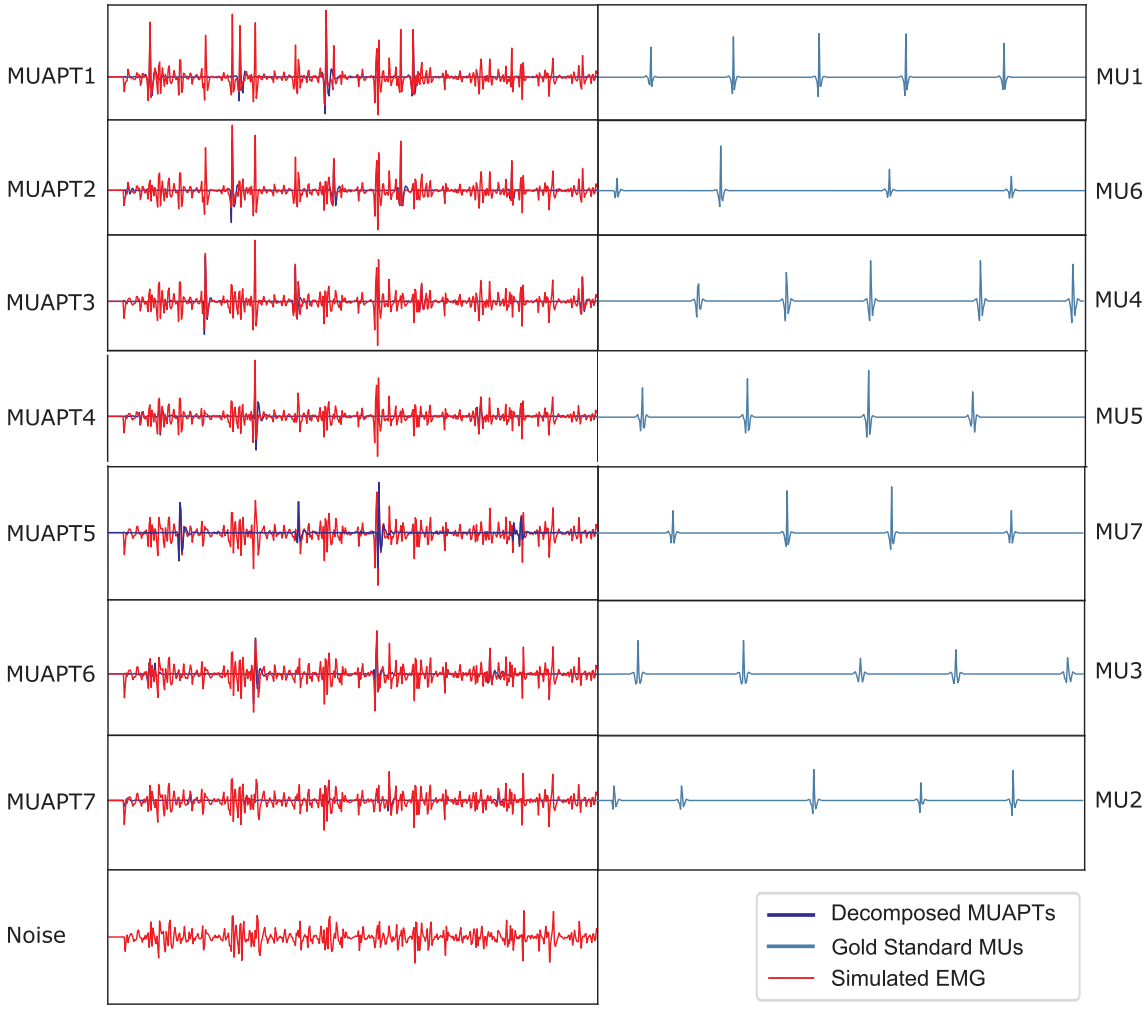

Fig. 6. Decomposition results using the peel-off strategy. From top to bottom are the MUAPTs decomposed one by one from the simulated iEMG using the peel-off strategy. On the left are the decomposed MUAPTs, and on the right are the corresponding gold-standard MUs.

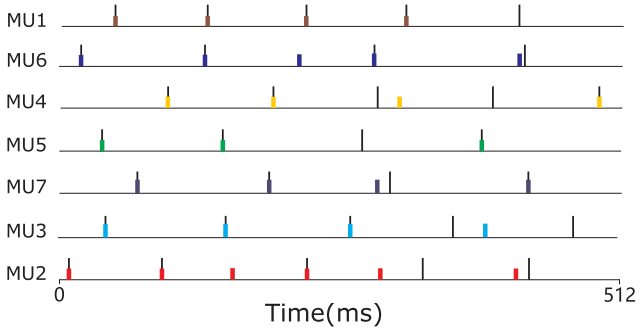

Fig. 7. Firing pattern of the decomposed MUAPTs compared with the gold-standard MUs. The black vertical lines denote the firing of the gold-standard MUs. The colourful vertical lines denote the firing of the decomposed MUAPTs. (For interpretation of the references to colour in this figure legend, the reader is referred to the web version of this article.)

firing of the motor unit but the generated MUAPTs does not capture it.

5.2.3. All-together Strategy

Penalties ϕ_0, ϕ_1, and ϕ_2 are set to 1, 2, and 0.5 for the all-together strategy. The decomposition results of the simulated iEMG signal using the all-together strategy are shown in Fig. 8. Seven out of the 64 generated MUAPTs with the largest absolute channel responses are shown and arranged according to their similarities to the gold-standard MUs. The simulated EMG signal and its approximation are shown at the top of the figure. The absolute value of the channel responses of the 64 batches of motor units are arranged from largest to smallest in the bottom-left panel of Fig. 8, in which a significant drop down of the value at the 7th motor unit can be observed. A drop down on the channel responses at the 7th MUAPT indicates that MUAPTs of the first 6 MUAPTs contribute significantly to the simulated EMG signal. The contribution of a MUAPT to the EMG signal is proportional to its absolute channel response.

The accuracy of the generated MUAPTs compared with that of the gold standard MUs is 59.46% with 22 true positives, 12 false negatives, and 3 false positives, as shown at the right bottom of Fig. 8. The firing time of the gold-standard motor unit with a small amplitude is not well captured by the generated MUAPTs, such as MU3 in Fig. 8. The average accuracy of the proposed approach in capturing firing time of the gold standard MUs is 53.02 ± 12.07% over the entire 30 s of the simulated iEMG signal.

The decomposition results of the simulated iEMG signal using the conventional method are shown in Fig. 9. Individual MUAPs are detected from the simulated iEMG signal and clustered according to their morphological characteristics. The accuracy of the conventional approach is 43.24% with 16 true positives, 16 false negatives, and 5 false positives, as shown in Fig. 9. The average accuracy of the conventional method is 37.24 ± 18.19% over the entire 30 s of the simulated iEMG signal.

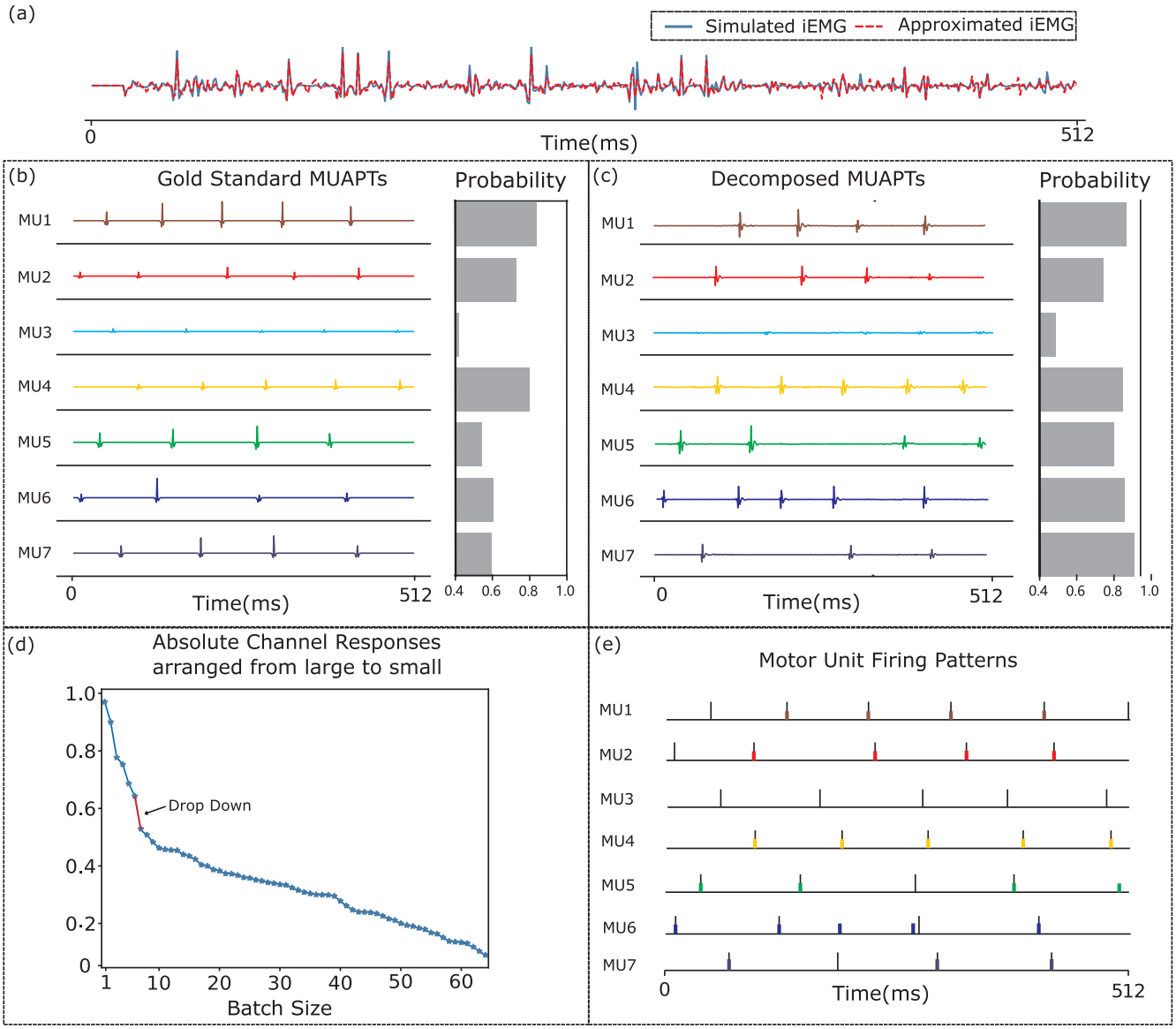

Fig. 8. Decomposition results of all-together strategy on the simulated iEMG signal. (a) The simulated iEMG signal to be decomposed and its approximation. (b) The gold-standard MUs and their probability of being real, as judged by the discriminator. (c) The decomposed o MUAPTs using the all-together strategy and their probability, as judged by the discriminator. (d) The absolute channel responses of the decomposed MUAPTs arranged from largest to smallest. The drop down indicates the sudden fall in the absolute channel responses. (e) Firing patterns of the decomposed MUAPTs compared with the gold-standard MUs. The black vertical lines denote the firing of the gold-standard MUs. The colourful lines denote the firing of the decomposed MUAPTs. (For interpretation of the references to colour in this figure legend, the reader is referred to the web version of this article.)

6. Discussion

Conventional methods decompose a iEMG signal into its MUAPTs by establishing an estimated distribution of MUAP characteristics, which depends on detecting enough individual MUAPs from the EMG signal. Therefore, it is difficult for conventional methods to decompose iEMG signals recorded by electrodes with large sensing areas or sampled at low frequencies due to superimpositions of MUAPs and the loss of MUAP morphological characteristics. In this paper, a decomposition approach based on Bayes' law and a generative adversarial network was proposed. The proposed approach achieved higher accuracy than conventional methods in decomposing simulated iEMG signals.

The power of the generative adversarial model in generating realistic MUAPTs is the basis for the proposed approach. The efficiency of a GAN in generating data has been validated in many fields, such as face generation (Liu et al., 2018) and speech synthesis (Kaneko et al., 2017). The deep architecture of the proposed WGAN-GP enables it to learn complex features of MUAPTs. The complex features learned by the WGAN-GP allow it to generate realistic MUAPTs with various morphological characteristics and firing patterns compared with the widely used Gaussian parametric model (Di et al., 2008). However, one limitation of the WGAN-GP is its lack of an objective metric to evaluate the quality of the instances generated by the generator (Vertolli and Davies, 2017); we used the area of overlap between the gamma distribution of the training set and the generated instances to evaluate it indirectly. The area of overlap was 85% for the proposed WGAN-GP, which means the generated instances covered 85% of the variability in the firing patterns in the training set. Empirically, the larger the area of overlap is, the better the quality of the generated instances. The area of overlap can be further improved by adding more MUAPTs to the training set or increasing the number of hidden layers in the WGAN-GP.

The decomposition loss function of the proposed approach is designed to maximize both the EMG model likelihood and the reality of the generated MUAPTs. The optimized MUAPTs are indeed the

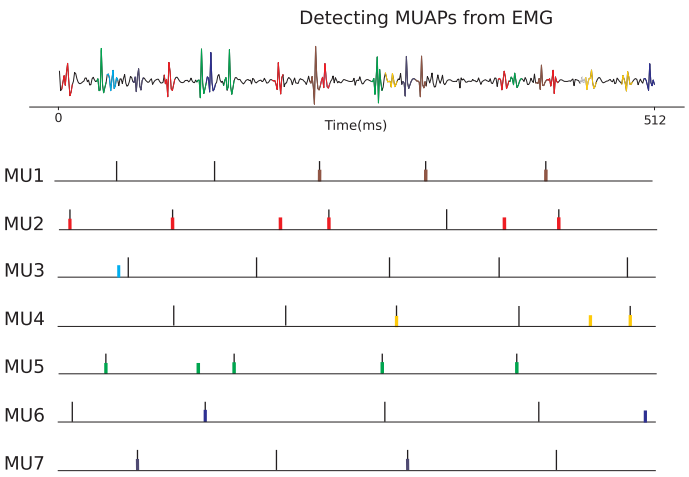

Fig. 9. Decomposition results of the conventional method on the first 512 ms of the simulated iEMG signal. The top of the figure shows the MUAPs detected from the iEMG. The bottom-left plot shows the firing pattern of the decomposed MUAPTs compared with the gold-standard MUs.The bottom-right plot shows the clustering of the detected MUAPs.

maximum likelihood estimates of the generated MUAPTs given the iEMG signal based on the decomposition loss function. A problem with maximum likelihood estimation is that an unlimited number of MUAPTs can be decomposed. To cope with this problem, a penalty to limit the channel responses is added to the loss function. The drop down in the channel responses is the result of the penalty, and it is used to determine the number of MUAPTs contributing significantly to the iEMG signal. The number of MUAPTs contributing significantly to the iEMG signal varies from a few to more than a hundred, as determined by muscle contraction levels (Parsaei et al., 2010). In this paper, an iEMG signal was decomposed at a batch size of 64, which is a compromise between decomposing enough MUAPTs and reducing memory usage.

Decomposing an iEMG signal sampled at a low frequency is difficult for conventional methods based on detecting and clustering MUAPs. The low sampling frequency has negative consequences on clustering the MUAPs. The state-of-the-art decomposition method based on detecting and clustering MUAPs has achieved an average accuracy of 87.23% on a simulated iEMG signal sampled at 30 kHz (Ren et al., 2018); nevertheless, the method only achieves a 37% accuracy on the simulated EMG signal sampled at 1 kHz in this paper. The decrease in accuracy reflects that conventional methods are highly dependent on the morphological characteristics of the MUAPs, which are greatly compromised in a 1 kHz sampled sEMG signal. The proposed approach depends on complex features learned by the WGAP-GP, which is not affected by the low sampling frequency. The errors of the proposed approach in capturing firing time of the gold-standard MUs are probably caused by the fact that the activities of the gold-standard MUs are not well covered by the training set, and the discriminator assigns a low probability of being real to the gold-standard MUs. The errors can be reduced to some extent by decreasing the penalty ϕ_1 in order to decrease the effect of the discriminator on the decomposition loss function; however, training the WGAN-GP to cover variabilities in the motor unit activities is a thorough solution to eliminate errors.

The proposed approach can be extended to decompose iEMG signal segments of any length. Currently, the segmentation length of 512 ms is adopted due to the memory limitations of the GPU. Increasing the segmentation length, to the best of our knowledge, can increase the performance of the proposed approach because the WGAN-GP will be able to obtain more information about the firing pattern of the MUs. This phenomenon is one of the benefits of the WGAN-GP as a module of deep learning to learn from very large amounts of data (Najafabadi et al., 2015).

The proposed approach, which allows the investigation of firing patterns and recruitment of motor units based on low-frequency iEMG signals recorded by electrodes with large sensing areas, has great potential in clinical applications, such as prosthetic limb control, rehabilitation performance evaluation, and neuromuscular disorder diagnosis.

7. Conclusion

An approach using a trained WGAN-GP to decompose iEMG signals to maximize both the EMG model likelihood and the reality of the decomposed MUAPTs was proposed. The approach achieved a 16% higher accuracy than the conventional method in capturing the firing regularities of the MUAPTs on simulated iEMG signals. The proposed approach can be used to study firing patterns and the recruitment of motor units in isometric muscle contractions based on fully implantable iEMG devices, and it has great potential in the applications of prosthetic limb control, rehabilitation performance evaluation, and neuromuscular disorder diagnosis. We are also working on hand-gesture classification based on the decomposed MUAPTs using our lab-made fully implanted devices (Tang et al., 2018), and some encouraging results have been obtained. The results will be reported in our next paper.

Declaration of Competing Interest

The authors declared that there is no conflict of interest.

Acknowledgements

The authors would like to thank all the staff running the EMGLAB website (http://www.emglab.net/) for their generous sharing of the software and data.

This work was supported by the Beijing Municipal Science and Technology Program (Grant No. Z181100003118007) and the National Natural Science Foundation of China (Grant Nos. 91648207 and 61673068).

Appendix A

The code of the proposed approach is available at https://github.com/sun2009ban/Single-Channel-sEMG-Decomposition. The data used in the paper are available at http://www.emglab.net/emglab/Signals/signals.php.

Appendix B

The code of the conventional method used to decompose the simulated EMG signal is available at https://github.com/sun2009ban/Spike_Sorting/tree/version2.0

Appendix C. Supplementary material

Supplementary data associated with this article can be found, in the online version, at https://doi.org/10.1016/j.jelekin.2019.07.015.

References

Mcgill, K.C., Lateva, Z.C., Marateb, H.R., 2005. Emglab: An interactive emg decomposition program. J. Neurosci. Methods 149 (2), 121–133.

Adrian, E.D., Bronk, D.W., 1928. The discharge of impulses in motor nerve fibres: Part I. Impulses in single fibres of the phrenic nerve. J. Physiol. 66 (1), 81–101.

Farina, D., Negro, F., 2015. Common synaptic input to motor neurons, motor unit synchronization, and force control. Exercise Sport Sci. Rev. 43 (1), 23–33.

Thompson, C.K., Negro, F., Johnson, M.D., Holmes, M.R., McPherson, L.M., Powers, R.K., Farina, D., Heckman, C.J., 2018. Robust and accurate decoding of motoneuron behaviour and prediction of the resulting force output. J. Physiol. 596 (14), 2643–2659.

Lefever, R.S., Luca, C.J.D., 1982. A procedure for decomposing the myoelectric signal into its constituent action potentials–part i: Technique, theory, and implementation. IEEE Trans. Bio-med. Eng. 29 (3), 149–157.

Luca, C.J.D., Adam, A., 1999. Decomposition and analysis of intramuscular electromyographic signals.

Mcdonnall, D., Hiatt, S., Smith, C., Guillory, K.S., 2012. Implantable multichannel wireless electromyography for prosthesis control. In: International Conference of the IEEE Engineering in Medicine & Biology Society.

Weir, R.F., Troyk, P.R., Demichele, G.A., Kerns, D.A., Schorsch, J.F., Maas, H., 2009. Implantable myoelectric sensors (imess) for intramuscular electromyogram recording. IEEE Trans. Biomed. Eng. 56 (1), 159–171.

Bergmeister, K.D., Vujaklija, I., Muceli, S., Sturma, A., Hruby, L.A., Prahm, C., Riedl, O., Salminger, S., Manzanoszalai, K., Aman, M., 2017. Broadband prosthetic interfaces: combining nerve transfers and implantable multichannel emg technology to decode spinal motor neuron activity. Front. Neurosci. 11, 421–435.

Negro, F., Muceli, S., Castronovo, A.M., Holobar, A., Farina, D., 2016. Multi-channel intramuscular and surface emg decomposition by convolutive blind source separation. J. Neural Eng. 13 (2), 026027.

Zhu, X., Zhang, Y., 2012. High-density surface emg decomposition based on a convolutive blind source separation approach. Conf. Proc. IEEE Eng. Med. Biol. Soc. 609–612.

Holobar, A., Zazula, D., 2004. Correlation-based decomposition of surface electromyograms at low contraction forces. Med. Biol. Eng. Comput. 42 (4), 487–495.

Holobar, A., Zazula, D., 2007. Multichannel blind source separation using convolution kernel compensation. IEEE Trans. Signal Process. 55 (9), 4487–4496.

Chen, M., Zhou, P., 2015. A novel framework based on fastica for high density surface emg decomposition. IEEE Trans. Neural Syst. Rehabil. Eng. 24 (1), 117–127.

De Luca, C.J., Chang, S.S., Roy, S.H., Kline, J.C., Nawab, S.H., 2015. Decomposition of surface emg signals from cyclic dynamic contractions. J. Neurophysiol. 113 (6), 1941–1951.

Stashuk, D., 2001. Emg signal decomposition: how can it be accomplished and used? J. Electromyogr. Kinesiol. 11 (3), 151–173.

Gerber, A., Studer, R.M., Figueiredo, R.J.D., Moschytz, G.S., 1984. A new framework and computer program for quantitative emg signal analysis. IEEE Trans. Biomed. Eng. 31 (12), 857–863.

Loudon, G.H., Jones, N.B., Sehmi, A.S., 1992. New signal processing techniques for the decomposition of emg signals. Med. Biol. Eng. Comput. 30 (6), 591–599.

Christodoulou, C.I., Pattichis, C.S., 1999. Unsupervided pattern recognition for the classification of emg signals. IEEE Trans. Biomed. Eng. 46 (2), 169–178.

Mcgill, K.C., Cummins, K.L., Dorfman, Leslie J., 1985. Automatic decomposition of the clinical electromyogram. IEEE Trans. Biomed. Eng. 32 (7), 470–477.

Stashuk, D., Bruin, D., 1988. H, Automatic decomposition of selective needle-detected myoelectric signals. IEEE Trans. Biomed. Eng. 35 (1), 1–10.

Etawil, H., Stashuk, D., 1996. Resolving superimposed motor unit action potentials. Med. Biol. Eng. Comput. 34 (1), 33–40.

Marateb, H.R., Muceli, S., McGill, K.C., Merletti, R., Farina, D., 2011. Robust decomposition of single-channel intramuscular emg signals at low force levels. J. Neural Eng. 8 (6), 066015.

Stoller, D., Ewert, S., Dixon, S., 2018. Adversarial semi-supervised audio source separation applied to singing voice extraction. In: 2018 IEEE International Conference on Acoustics, Speech and Signal Processing (ICASSP), pp. 2391–2395.

Subakan, Y.C., Smaragdis, P., 2018. Generative adversarial source separation. In: 2018 IEEE International Conference on Acoustics, Speech and Signal Processing (ICASSP), pp. 26–30.

De Luca, C.J., Forrest, W.J., 1973. Some properties of motor unit action potential trains recorded during constant force isometric contractions in man. Kybernetik 12 (3), 160–168.

Holobar, A., Farina, D., 2014. Blind source identification from the multichannel surface electromyogram. Physiol. Meas. 35 (7), 143–165.

EricZiegel, Kendall"s, 1994. advanced theory of statistics, vol. 1: Distribution theory. Technometrics 31 (1), 128.

Goodfellow, I.J., Pouget-Abadie, J., Mirza, M., Xu, B., Warde-Farley, D., Ozair, S., Courville, A., Bengio, Y., 2014. Generative adversarial nets. In: International Conference on Neural Information Processing Systems, pp. 2672–2680.

Radford, A., Metz, L., Chintala, S., 2015. Unsupervised representation learning with deep convolutional generative adversarial networks. Comput. Sci.

Pascual, S., Bonafonte, A., Serrà, J., 2017. Segan: Speech enhancement generative adversarial network. In: *Proceedings of Interspeech*, pp. 3642–3646.

Rajeswar, S. Subramanian, S., Dutil, F., Pal, C., Courville, A., 2017. Adversarial generation of natural language. In: *Proceedings of the 2nd Workshop on Representation Learning for NLP*, pp. 241–251.

Yadav, A., Shah, S., Xu, Z., Jacobs, D., Goldstein, T., 2017. Stabilizing adversarial nets with prediction methods, arXiv preprint arXiv:1705.07364.

Che, T., Li, Y., Jacob, A.P., Bengio, Y., Li, W., 2016. Mode regularized generative adversarial networks.

Arjovsky, M., Chintala, S., Bottou, L., 2017. Wasserstein gan, arXiv preprint arXiv:1701.07875.

Gulrajani, I., Ahmed, F., Arjovsky, M., Dumoulin, V., Courville, A., 2017. Improved training of wasserstein gans. In: *Advances in Neural Information Processing Systems*, pp. 5767–5777.

Mueller, J.W., Jaakkola, T., 2015. Principal differences analysis: interpretable characterization of differences between distributions. In: Advances in Neural Information Processing Systems, pp. 1702–1710.

Arora, S., Zhang, Y., 2017. Do gans actually learn the distribution? an empirical study. arXiv preprint arXiv:1706.08224.

McGill, K., 2015. [online dataset r001 and r005, available at <http://www.emglab.net>].

Xiang, S., Li, H., 2017. On the effects of batch and weight normalization in generative adversarial networks. arXiv preprint arXiv:1704.03971.

Hamilton, W.A., Stashuk, D., 2005. Physiologically based simulation of clinical emg signals. IEEE Trans. Biomed. Eng. 52, 171–183.

Arthur, D., Vassilvitskii, S., 2007. k-means++: the advantages of careful seeding, Proceedings of the Eighteenth Annual ACM-SIAM Symposiumon Discrete algorithms. Soc. Ind. Appl. Math. 11 (6), 1027–1035.

Liu, X., Xie, C., Kuang, H., Ma, X., 2018. Face aging simulation with deep convolutional generative adversarial networks. In: International Conference on Measuring Technology and Mechatronics Automation, pp. 220–224.

Kaneko, T., Kameoka, H., Hojo, N., Ijima, Y., Hiramatsu, K., Kashino, K., 2017. Generative adversarial network-based postfilter for statistical parametric speech synthesis. In: IEEE International Conference on Acoustics, Speech and Signal Processing, pp. 4910–4914.

Di, G., Carpentier, E.L., Farina, D., Idier, J., 2008. Unsupervised bayesian emg decomposition algorithm using tabu search. In: International Symposium on Applied Sciences on Biomedical and Communication Technologies, pp. 1–5.

Vertolli, M.O., Davies, J., 2017. Image quality assessment techniques show improved training and evaluation of autoencoder generative adversarial networks. arXiv preprint arXiv:1708.02237.

Parsaei, H., Stashuk, D.W., Rasheed, S., Farkas, C., Hamilton-Wright, A., 2010. Intramuscular emg signal decomposition. Crit. Rev. Biomed. Eng. 38 (5), 357–368.

Ren, X., Zhang, C., Li, X., Yang, G., Potter, T., Zhang, Y., 2018. Intramuscular emg decomposition basing on motor unit action potentials detection and superposition resolution. Front. Neurol. 9.

Najafabadi, M.M., Villanustre, F., Khoshgoftaar, T.M., Seliya, N., Wald, R., Muharemagic, E., 2015. Deep learning applications and challenges in big data analytics. J. Big Data 2 (1), 1–21.

Tang, R., Lv, X., Sun, W., Dai, C., Zhang, M., Xin, L., She, H., Zhang, X., Lang, Y., Zhu, J., 2018. A fully implantable wireless neural interface for simultaneous recording from multiple sites of peripheral nerves in free moving animal. IEEE International Conference on Cyborg & Bionic Systems.

Wentao Sun received the B.S. degree in Mechatronical engineering from Beijing Institute of Technology, Beijing, China, in 2013, where he continues to pursue the Ph.D. degree with the School of Mechatronical Engineering. He is an active member of deep learning and open-source community. His current research focuses on using deep learning tools to improve the control of the prosthetic hands.